The 9th European Congress on Computational Methods in Applied Sciences and Engineering
ECCOMAS Congress 2024
3–7 June 2024, Lisboa, Portugal

INFLUENCE OF FREE-STREAM TURBULENCE AND DISCRETE ROUGHNESS ELEMENTS ON THE RECEPTIVITY OF TWO-DIMENSIONAL BOUNDARY LAYERS

Emilio López Figueiras[1,2], Daniel Rodríguez[2] and Jean-Baptiste Gouriet[1]

[1] von Karman Institute for Fluid Dynamics
Waterloosesteenweg 72, 1640 Sint-Genesius-Rode, Belgium
e-mail: secretariat@vki.ac.be, www.vki.ac.be

[2] School of Aeronautics ETSIAE, Universidad Politécnica de Madrid
Plaza Cardenal Cisneros 3, 28040 Madrid, Spain
email: info.aeroespacial@upm.es, www.upm.es

Key words: Receptivity, Transition to Turbulence, Discrete Roughness Element, Free-stream Turbulence, Direct Numerical Simulation, Flat Plate

Summary. The receptivity of a two-dimensional boundary layer flow developing on a flat plate with a super-elliptical leading edge to incoming disturbances in the presence of a discrete roughness element (DRE) is studied by direct numerical simulation. The DRE is a truncated cylinder with height k and fixed diameter. Its height is varied to cover a parameter space defined by the ratio of the element height to the local boundary layer displacement thickness k/δ^* and the Reynolds number based on the element height, Re_{kk}. Under the conditions simulated, in the absence of externally-imposed disturbances, steady flows are recovered. Two sources of disturbances are then considered: a localized volumetric forcing analogous to a suction/blowing strip that introduces plane monochromatic Tollmien-Schlichting (T-S) waves upstream of the DRE, and synthetic isotropic free-stream turbulence (FST) imposed as an inlet condition upstream of the leading edge. Two different dimensionless temporal frequencies of the T-S waves, $F = 90 \times 10^{-6}$ ($\omega = 0.21$) and $F = 120 \times 10^{-6}$ ($\omega = 0.29$), two DRE heights, $k = 0.3\delta^*$ ($Re_{kk} = 50$) and $k = 0.5\delta^*$ ($Re_{kk} = 138$) and the turbulence intensities $Tu = 0.03\%$ and $Tu = 0.3\%$, are combined in multiple test-cases and analysed through the amplification factor of the resulting disturbances.

1 INTRODUCTION

In the search of the aviation industry for more efficient aircraft that reduce the carbon footprint of commercial flights, the improvement in aerodynamic efficiency is a key goal that can be achieved by minimizing the aerodynamic drag of the wings. In this sense, the most important contribution to aerodynamic drag is produced by skin friction due to turbulent flow. Hence, special efforts are put into the delay or suppression of the processes that lead to the flow transition to turbulence, increasing the fraction of the wing surface that is under laminar flow conditions. The design of such natural laminar flow strategies requires a deep understanding of the complete physical processes that lead to transition. Following Morkovin [1], the relevant

laminar-turbulent transition scenarios in boundary layer flows are initiated with the penetration or inception of flow disturbances within the boundary layer, in a process named receptivity. This can occur through wall imperfections (discontinuities or roughness), leading-edge curvature, vibrations, free-stream disturbances that impinge the aerodynamic surface, and generally via a combination of two or more of them. The receptivity process determines the nature, spatial structure and amplitude of the initial boundary-layer disturbances, prior to their amplification by hydrodynamic instability mechanisms.

The receptivity of two-dimensional boundary layers in incompressible flows has received continuous attention for several decades, as it constitutes the simplest configuration of relevance to transition on wings. Modal instability in two-dimensional boundary layers under favorable and moderately-adverse pressure gradients is dominated by Tollmien-Schlichting (T-S) waves. Their relatively small growth rates result in a linear growth phase that may extend over a significant portion of the airfoil before non-linear phenomena become relevant, which explains the broad success of transition prediction methods based on the accumulated amplification, like the e-to-the-N method[2, 3], for this kind of flows. However, despite of the relatively simple linear amplification phase, these methods rely on experimental calibration of the transition N-factor to account for the impact of free-stream turbulence intensity, wall roughness and other aspects related to receptivity.

With the aim of minimizing the impact of surface discontinuities in flat-plate experiments, Lin et al. [4] introduced the so-called "modified super-elliptic leading edge" geometry which results in a smooth continuous surface joining the leading edge to the plate with zero curvature at the joint. They used this geometry to study experimentally the receptivity to externally-controlled acoustic disturbances. For the same geometry, [5] or [6] did numerical analyses of the receptivity to inflow disturbances of different types. The latter analyzed the boundary-layer receptivity to three-dimensional vortical perturbations, triggering a streaky pattern of the disturbance streamwise velocity inside the boundary layer for the zero-frequency streamwise vorticity, and getting T-S modes for the high-frequency spanwise vorticity modes.

While the receptivity process is significantly weaker, it is recognized that free-stream turbulence can penetrate in the boundary layer even in the absence of wall discontinuities, irregularities or vibration, due to its weak non-parallelism. Jacobs and Durbin [7] or Brandt et al. [8], went further in the modeling of the inlet perturbations and studied the transition of boundary layers after imposing isotropic free-stream turbulence at the inlet boundary, where the turbulence intensity and the turbulence integral length scale are used as control parameters. In both works the turbulent inflow is constructed using the continuous spectrum of the linearized Navier-Stokes equations [9], together with analytical models of the turbulent kinetic energy spectrum.

The receptivity to free-stream disturbances is remarkably increased by the presence of surface imperfections and roughness; early works illustrate that the presence of a discrete roughness element (DRE) of small but comparable size to the local boundary layer thickness can enhance the penetration of external disturbance so as to render the effect of boundary-layer non-parallelism negligible. The experimental work of Plogmann et al. [10] introduced the classification of the roughness elements according to the height of the element k relative to the local displacement thickness δ^*, as small ($k/\delta^* < 0.2$), when they produce linear receptivity with k; medium ($0.2 < k/\delta^* < 1.0$), that generate non-linear receptivity and a qualitative change in the steady flow topology in the form of a horseshoe-shaped vortex upstream of the roughness element; and large ($k/\delta^* > 1.0$), which produce bypass transition just around or shortly downstream of the

roughness element. The numerical study made by Bucci et al. [11] included isotropic free-stream turbulence and studied the effect that several DRE and turbulence parameters have on the dynamics of a two-dimensional incompressible boundary layer over an infinite flat plate. It was concluded that the roughness Reynolds number (Re_{kk}), the aspect ratio of the roughness element (η), the ratio between the roughness height and the boundary layer displacement thickness (k/δ^*), and the free-stream turbulence intensity (Tu) altogether have an impact on the stability and transition of two-dimensional boundary layers. Turbulence intensities between 0.06% and 0.09% produce a meaningful destabilizing effect on the wake of the roughness element. The work by Bucci et al. [11] also proposed the development of a more sophisticated transition diagram than the one proposed by von Doenhoff [12], where only k/δ^* and Re_{kk} are considered. In Weingartner et al. [13] the analysis is focused on a flow visualization study of isolated roughness elements with different η and Re_{kk}. In sub-critical regimes ($Re_{kk} \lesssim 750$) all the aspect ratios produced a varicose (symmetric) disturbance pattern, while it was sinuous (anti-symmetric) in the range of $0.7 \leqslant \eta \leqslant 1.2$. The influence of a small discrete roughness element on the evolution of two-dimensional T-S waves was studied experimentally in [14], where a disturbance source in placed upstream of the roughness element. The results showed a weak flow distortion and scattering of the wave into oblique ones for $k/\delta^* = 0.2$ and a quadratic variation of the wave scattering with respect to k for a roughness height well below the displacement thickness.

Most works in the literature that address two-dimensional boundary layers either consider the leading-edge or the discrete roughness element in the presence of incoming vortical disturbances, but not both simultaneously. Further, most works studying the impact of DREs consider either the limit cases of small or large roughness heights, while the range of medium-height elements (k between 20% and 70% of the boundary-layer displacement thickness) is underrepresented in the literature. The combination of synthetic free-stream turbulence and the analysis of its effect on the receptivity in the presence of a leading-edge and a roughness element is also a missing point in the literature. Only the recent work by Vincentiis et al. [15] combines these aspects for a swept-wing case with a three-dimensional boundary layer. Including all these features in the same work could help to give more detail and depth to the transition diagram by Von Doenhoff et al. [12]. This is the objective of the present work.

This work addresses the receptivity analysis of incompressible, nominally two-dimensional boundary layers to free-stream turbulence, discrete roughness elements and their interaction, using direct numerical simulations. The geometry studied is a semi-infinite flat plate with a modified super-ellipse as a leading edge. A cylindrical discrete roughness element is introduced on the flat plate at streamwise locations contained between the first and the second branch of the neutral instability curve for plane T-S waves, and with heights that cover the range from small to large roughness regimes. Synthetic free-stream turbulence is imposed at the inlet following the methodology proposed by Schlatter [16]. Finally, a volumetric forcing term is used to mimic the effect of a suction/blowing slot or a vibrating ribbon and excite plane T-S waves upstream of the DRE. This methodology allows to study the interaction of different relevant aspects of the receptivity process in the same computational set-up.

2 METHODOLOGY

Direct numerical simulations (DNS) are carried on using the Spectral Element Method implemented in the open-source code Nek5000 [17], in which the order of the polynomial used to

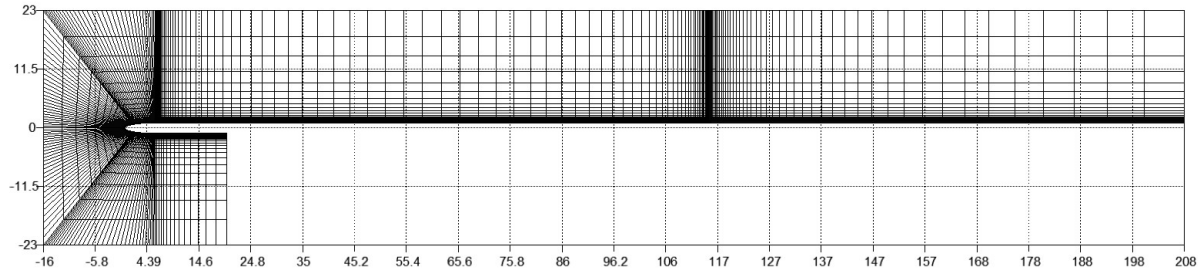

Figure 1: General view of the computational domain and mesh, including the DRE (at $x = 115$). The number of elements in the spatial mesh is reduce to ease its visualization.

approximate the velocity and pressure fields within each element takes the form $\mathbb{P}_N - \mathbb{P}_{N-2}$, respectively. Unless stated otherwise, the polynomial order is chosen as $N = 7$ for the simulations presented herein. Following the custom practice in hydrodynamic instability, separate simulations are performed for the computation of the base flows (two-dimensional or three-dimensional steady flows) and the three-dimensional linear disturbances developing upon them. Parabolized stability equations (PSE) calculations are also performed to compute the neutral curve for Tollmien-Schlichting (T-S) waves that is used as reference for placing the discrete roughness element.

2.1 Base geometry and numerical domain

The geometry of interest is shown in figure 1. A semi-infinite flat plate is considered in which the leading edge has the shape of the modified super-ellipse (MSE)

$$\left(\frac{y}{b}\right)^2 = 1 - \left(\frac{a-x}{a}\right)^p, \tag{1}$$

where

$$p = 2 + \left(\frac{x}{a}\right)^2, \tag{2}$$

and a and b are the major and minor semi-axes of the ellipse respectively. The modified super-ellipse reduces the geometrical discontinuity in the junction between the leading edge and the flat plate, with the aim of minimizing its influence on the boundary layer receptivity to free-stream incoming disturbances. The aspect ratio is taken as $AR \equiv \frac{a}{b} = 6$. The minor semi-axis b is used to non-dimensionalize all lengths throughout the paper.

The downstream length of the computational domain is defined based on the displacement thickness of the two-dimensional boundary layer that develops on the upper side of the flat plate. An initial estimate of the domain length is done assuming the Blasius self-similar solution for a zero-pressure-gradient boundary layer, and obtaining the $x-$coordinate corresponding to a Reynolds number based on the displacement thickness $Re_{\delta^*} \approx 1100$, which is downstream of the second branch of the neutral curve for T-S waves for most of the relevant frequencies. This estimation is later compared with the actual base flow computation.

2.2 Base flow computation

Base flow solutions are computed by solving the unsteady incompressible Navier-Stokes equations using Nek5000. Other than the downstream extension, the computational domain mimics the one used by Schrader et al. [6]: to reduce the computational cost, the computational domain used in Nek5000 is shortened in its lower half. The inlet, top and bottom boundaries, that would need to be located at a far distance to accommodate the flow displacement exerted by the solid, are instead truncated at a relatively short distance, as shown in figure 1. Velocity distributions are imposed as Dirichlet conditions at the truncated domain boundaries, that were computed using a numerical simulation on a much larger domain. The minor semi-axis b of the super-ellipse and the free-stream velocity U_∞ are taken as reference quantities for the dimensionless form. The kinematic viscosity is chosen such that the reference Reynolds number $Re_b = U_\infty b/\nu = 2400$.

No slip is imposed at the solid walls, while periodic boundary conditions are set for the spanwise direction. The outlet boundaries have a special treatment, minimizing the dependency of the solution on the length of the lower part and ensuring that the flow field is symmetric over the upper and the lower surface of the flat plate. The solution proposed in [18] solves that issue, as it defines natural boundary conditions at both outlet boundaries, imposing an ambient pressure profile in the lower half. This pressure profile is obtained from the steady base flow obtained for the upper-half of the domain, taking the pressure profile at the same x location as the lower boundary.

2.3 Isotropic free-stream turbulence

Synthetic free-stream turbulence (FST) is modeled here using a similar procedure to Schlatter [16], which models in-flight or wind-tunnel turbulence conditions described by a prescribed turbulent kinetic energy spectra $E(k)$, where E is the portion of the TKE associated with the spatial wavenumber k. The method is based on the continuous spectrum of vorticity perturbation solutions of the linearized Navier-Stokes equations for uniform flow, which can be written as a superposition of Fourier modes on the three spatial directions and time:

$$\mathbf{u}(x,y,z) = \sum_{\mathbf{k}=(\omega,\gamma,\beta)} A(k)\hat{\mathbf{u}}(\omega,\gamma,\beta)e^{i(\Re\{\alpha(\omega,\gamma,\beta)\}x+\gamma y+\beta z-\omega t)}, \tag{3}$$

where $\mathbf{u}$ is the velocity perturbation vector, $\mathbf{k}$ is the wave-vector; α, γ, and β are the wavenumbers in the streamwise, wall-normal and spanwise directions respectively, i.e. $k = \sqrt{\alpha^2+\beta^2+\gamma^2}$; ω is the time frequency, $A(k)$ are the amplitudes and $\hat{\mathbf{u}}$ are the normalized eigenfunctions of the continuous spectrum.

The isotropic turbulence is generated by dividing the wavenumber space k into N_s concentric shells. The magnitude of the radius of each of them is the wavevector magnitude k and it is associated to an amplitude within the the modeled turbulence spectrum $E(k)$:

$$A(k) = \sqrt{\frac{2E(k)\Delta k}{N_v}}, \tag{4}$$

where Δk defines the discretization of the wavenumber space and N_v is the number of independent vectors of magnitude k considered. In this work, the homogeneity is achieved by picking

$N_v = 20$ points regularly distributed as the vertices of a regular dodecahedron, which is increased by adding a second dodecahedron symmetric to the original with respect to the γ-plane. Each dodecahedron is rotated a random angle to ensure that the turbulence is isotropic.

The amplitudes for the chosen wavenumbers match the the von Kármán energy spectrum:

$$E(k) = Tu^2 U_\infty^2 L_I \frac{1.606(kL_I)^4}{(1.350 + (kL_I)^2)^{17/6}}, \tag{5}$$

where L_I is the integral length scale, U_∞ is the free-stream velocity and Tu is the turbulent intensity.

In this work, the synthetic FST is imposed as a boundary condition at the inlet and upper and lower boundaries, and considers the turbulent spectrum between $k_{min} = 0.23$ and $k_{max} = 3$, divided in 80 shells, which includes a relevant range of frequencies according to preliminary PSE computations that will be introduced below. The range of turbulence intensity considered in the study lies between 0% (no inflow FST) and 0.3%. The integral length scale chosen is $L_I = 2.0$ to ensure that scales with the maximum energy of the von Kármán spectrum lay on the range of the spectrum generated.

2.4 Discrete roughness element

A cylindrical discrete roughness element (DRE) is added to upper side of the flat plate geometry. Its geometrical features and location are based on the experiments by de Paula et al. [14]. A reference case is considered in which the DRE is located at a streamwise position corresponding to a Reynolds number based on the displacement thickness $Re_{\delta^*} = U_\infty \delta^*(x)/\nu = 920$ and the height of the DRE $k = 0.3\delta^*$.

A matrix of cases is defined by varying the height of the roughness element. Two dimensionless parameters are monitored, namely $Re_{kk} = U_k k/\nu$, where U_k is the flow velocity at the DRE height in the "clean" configuration (i.e. without the roughness element) and the ratio k/δ^*. The DRE heights chosen for this work are within the medium-height range defined in the literature, i.e. $k = 0.3\delta^*$ and $k = 0.5\delta^*$, with $Re_{kk} = 50$ and $Re_{kk} = 138$ respectively.

2.5 Forced Tollmien-Schlichting waves

Tollmien-Schlichting waves are excited in the flow field with the application of a volumetric forcing term $f(x, y, t)$ applied to the y-momentum equation and given by the expression

$$f(x, y, t) = A_f \cdot \exp\left(-\left(\frac{x - x_c}{s_x}\right)^2 - \left(\frac{y - y_c}{s_y}\right)^2\right) \cos(\omega t), \tag{6}$$

where A_f is the amplitude of the forcing term, with a value of 0.8% of the free-stream velocity; x_c and y_c are the coordinates of the forcing strip; $s_y = \delta_c^*$ and $s_x = 2.5 s_y$. The streamwise coordinate x_c is set to correspond to $Re_{\delta^*} = 700$ and $y_c = 1$, which places the actuator on the wall surface. The dimensionless circular frequency ω is defined as $\omega = Re_b F$, where F is the dimensionless frequency typically used in the characterization of T-S waves: $F = 2\pi f \nu / U_\infty^2$.

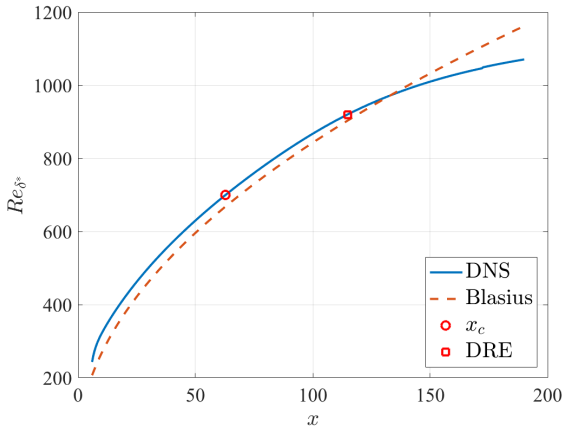

Figure 2: Evolution of the Reynolds number based on the displacement thickness Re_{δ^*} along the flat-plate chord.

3 RESULTS

3.1 Base flow without roughness element

A two-dimensional simulation of the "clean" flat plate geometry with super-elliptic leading edge, but without the roughness element, free-stream turbulence or T-S waves is carried out to assess the quality of the computational mesh, evaluate the development of the boundary layer flow, and define the location of the actuator x_c and discrete roughness element, which are based on the displacement thickness distribution.

Figure 2 shows the Reynolds number based on the displacement thickness distribution $\delta^*(x)$ corresponding to the numerical simulation, compared to the self-similar Blasius distribution. The presence of the leading edge leads to a departure of the flow from the self-similar one: first, the streamlines are curved following the super-ellipse until $x = 6$, which is the junction between the LE and the flat plate. The displacement thickness is only computed for $x > 6$. Second, the curvature of the streamlines and non-parallelism leads to a velocity maximum at the end of the boundary layer, that then reduces on the wall-normal direction towards the free-stream value. To take this into account, the boundary layer thickness is computed as:

$$\delta^*(x) = \int_0^{y_{u,max}} \left(1 - \frac{U(x,y)}{U(x,y_{u,max})}\right) dy. \tag{7}$$

This definition converges monotonically towards the parallel-flow definition (where $y_{u,max} \to \infty$) as the boundary layer develops.

As shown by figure 2, the computed base flow has a small deviation from the Blasius self-similar solution. The actual Re_{δ^*} distribution is used to locate the actuator and the roughness elements. Following De Paula et al. [14], the actuator generating T-S waves is located at $Re_{\delta^*} = 700$, corresponding to $x_c = 65$, and the DRE at $Re_{\delta^*} = 920$, corresponding to $x = 115$. Based on the computed Re^*_δ distribution, the outlet boundary is placed at $L = 200$, to ensure a $Re_{\delta^*} \geq 1100$ at the end of the domain.

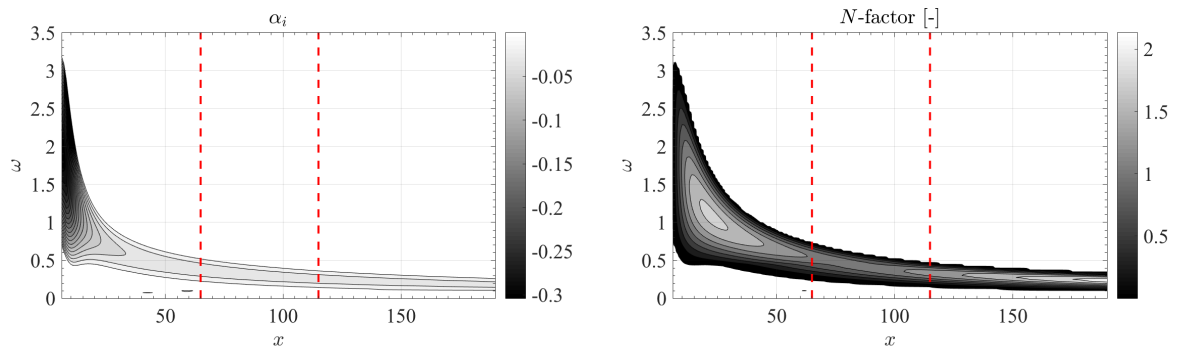

Figure 3: PSE results for T-S waves on the 2D boundary layer. Left: spatial growth rate $-\alpha_i$. Right: $N-$factor. The vertical dashed lines show the location of T-S actuator and the baseline DRE, for reference.

3.2 Amplification of T-S waves by the 2D boundary layer

Prior to the receptivity analysis involving free-stream turbulence and a DRE, PSE calculations are performed using a well-validated code [19, 20]. The calculations are initiated at $x = 6$, where the flat plate section starts, making it unnecessary to account for the wall curvature near the leading edge. The results for plane T-S waves are shown in figure 3. The left panel shows the spatial growth rate. Plane T-S waves are found to be linearly unstable already at $x = 6$, presumably as a consequence of the base flows streamlines curvature stemming from the leading edge geometry. This region of upstream instability is located well upstream the expected location of the first branch of the neutral curve for the Blasius boundary layer, that occurs around $Re_{\delta^*} \approx 500$ ($x \approx 30$ for the present flow), and for notably higher frequencies. This amplification rate is reduced one order of magnitude from $x = 6$ to $x = 65$, where the T-S actuator is located in the DNS set-up, and the unstable frequency range becomes considerably narrower and for lower frequencies, consistent with what is expected for a Blasius boundary layer.

The right panel in figure 3 shows the integrated amplification in terms of the N-factor:

$$N(x, \omega) = \int_{x_n}^{x} -\alpha_i(x', \omega) dx', \tag{8}$$

where x_n is the coordinate where the T-S wave becomes unstable for each ω. For those frequencies that are unstable at the beginning of the integration domain for PSE calculations, $x_n = 6$. The N-factor contours show that the high-frequency waves that are unstable near the leading edge are quickly damped downstream. Conversely, the comparatively lower frequencies that are typical of Blasius boundary layer instability remain amplified until the domain outlet.

Overall, the N-factor computed in this domain remains below $N = 2.5$, which corresponds to very small accumulated amplifications and are adequate for a study of the receptivity processes.

DNS calculations were performed including the plane T-S waves at two relevant frequencies, $F = 90 \times 10^{-6}$ ($\omega = 0.21$) and $F = 120 \times 10^{-6}$ ($\omega = 0.29$), as perturbations of the Linearized Navier-Stokes equations convected downstream by the precomputed base flow.

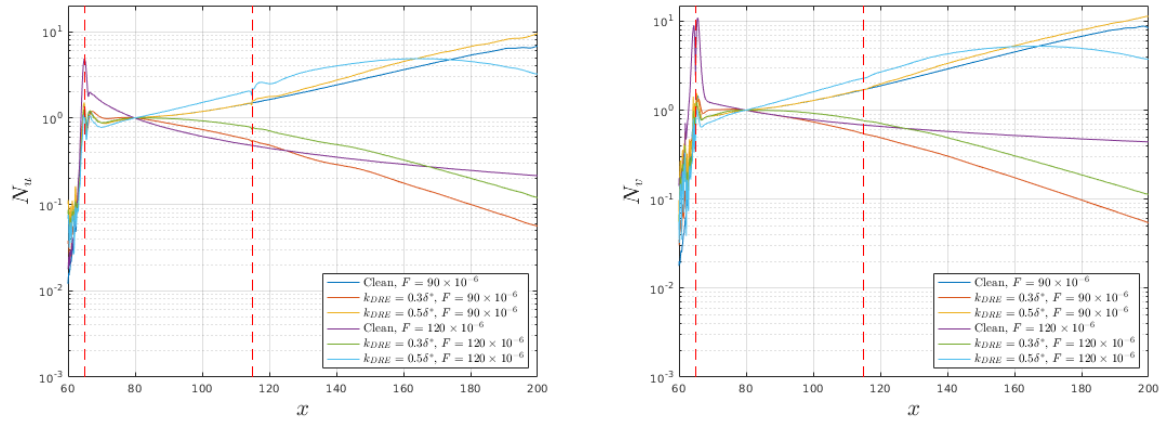

Figure 4: Amplification factor of the the components of the perturbations generated by the forced T-S waves in different scenarios. The vertical dashed lines show the location of T-S actuator and the baseline DRE. Left: Amplification factor of the streamwise velocity, N_u. Right: Amplification factor of the wall-normal velocity, N_v.

3.3 Receptivity of the 2D boundary layer to a discrete roughness element and forced T-S waves

A new set of DNS calculations are carried out for cases including a DRE with two different roughness heights, $k = 0.3\delta^*$ ($Re_{kk} = 50$) and $k = 0.5\delta^*$ ($Re_{kk} = 138$). The resulting flow field serves as the base flow for computations with the Linearized Navier-Stokes equations where T-S waves are introduced as previously described.

Figure 4 shows the differences in the amplification factors of the perturbations for the cases of interest after a significant period of time. More precisely, the maximum of the absolute value of the velocity components in the wall-normal direction is taken for each x-coordinate position. Afterwards, it is normalized with a reference value taken at $x = 80$. The results are plotted to compare the effect over the perturbation field of the reference frequencies and roughness element heights. Both velocity components have similar behaviour in terms of their respective amplification factor, and "clean" configurations show opposite behaviours for each T-S wave frequency, as the amplitude grows for the case at $F = 90 \times 10^{-6}$ ($\omega = 0.21$) and decays for the T-S wave at $F = 120 \times 10^{-6}$ ($\omega = 0.29$).

Focusing on the cases with a T-S wave at $F = 90 \times 10^{-6}$ ($\omega = 0.21$), the "clean" case and the case with DRE of $k = 0.5\delta^*$ ($Re_{kk} = 138$) increase in amplitude, with a slight increase of the growth rate downstream of the DRE for the DRE case. The DRE case with $k = 0.3\delta^*$ ($Re_{kk} = 50$), on the other side, shows a gradual decrease in amplitude all along the domain length.

The cases including a T-S wave at $F = 120 \times 10^{-6}$ ($\omega = 0.29$) have a negative growth rate for the "clean" and $k = 0.3\delta^*$ ($Re_{kk} = 50$) configurations, with a bigger decline in amplitude downstream of $x \approx 170$ for the case with a DRE. The addition of a DRE with $k = 0.5\delta^*$ ($Re_{kk} = 138$) causes a great impact on the behaviour of the wave, which is growing in amplitude along the whole domain.

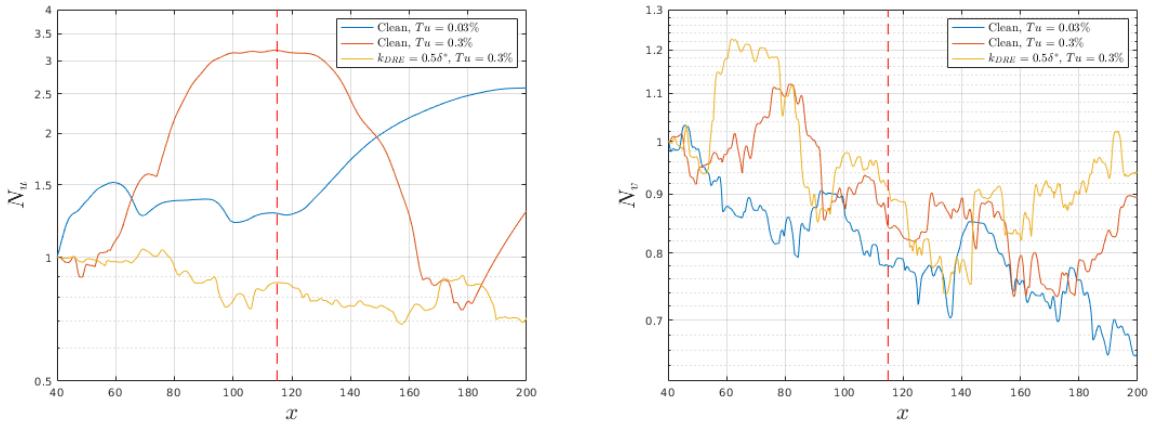

Figure 5: Amplification factor of the the components of the perturbations generated by the isotropic FST in different scenarios. The vertical dashed lines show the location of T-S actuator and the baseline DRE. Left: Amplification factor of the streamwise velocity N_u. Right: Amplification factor of the wall-normal velocity N_v.

3.4 Receptivity of the 2D boundary layer to isotropic free-stream turbulence

For the study of the receptivity of the boundary layer developed over the flat plate to isotropic free-stream turbulence, two turbulence intensities of $Tu = 0.03\%$ and $Tu = 0.3\%$ are considered.

The same analysis as for the case with T-S waves was done for the case with isotropic FST, taking the streamwise position $x = 40$ as the reference for normalization.

In these cases, there is a great difference in the behaviour of each velocity component, as the amplification factors are greater than 1 for the streamwise velocity component, while the amplitude of the wall-normal component is decreasing in most of the domain length.

Comparing the cases under "clean" configuration, the FST with $Tu = 0.03\%$ has a smaller value of N_u overall, although both turbulence intensities show a positive growth rate. The addition of a DRE with $k = 0.5\delta^*$ ($Re_{kk} = 138$) seems to have a stabilizing effect, as the amplitudes decay along the whole domain length.

4 CONCLUSIONS

The simulations carried out during the present work served as a basis to establish a matrix of test cases that allowed the analysis of the receptivity of a two-dimensional boundary layer developed over a flat plate. The parameters under consideration for the analysis were the dimensionless circular frequency for the cases including a T-S actuator on the flat plate surface, the turbulence intensity of isotropic free-stream turbulence introduced as an inlet condition and the height of a DRE placed on the flat plate surface, at a reference streamwise location.

The preliminary results served as a guide for the location and size of the discrete roughness element and gave initial estimations of the stability of the T-S waves developing over a base flow and of the most convenient frequencies to be included in the synthetic FST.

From the analysis of the amplification factor of the perturbations generated by the T-S actuator, it is concluded that the addition of the smaller DRE, with $k = 0.3\delta^*$ ($Re_{kk} = 50$),

to the case at low frequency, $F = 90 \times 10^{-6}$ ($\omega = 0.21$), stabilizes the perturbation field. On the other side, the higher DRE, with $k = 0.5\delta^*$ ($Re_{kk} = 138$), has a destabilizing effect for the perturbations obtained from the T-S wave at $F = 120 \times 10^{-6}$ ($\omega = 0.29$).

Finally, the addition of isotropic FST at the inflow of the "clean" case with very low values of Tu increases the amplitude of the perturbations in comparison with addition of the T-S actuator. In these scenarios, the presence of the DRE with $k = 0.5\delta^*$ ($Re_{kk} = 138$) stabilizes the perturbations shifting the sign of their growth rates and reducing their amplitudes in general.

Acknowledgments

This work is funded by European Union's Horizon 2020 research and innovation programme under the Marie Skłodowska Curie grant agreement No 955923-SSECOID. D.R. is funded by the projects MIXSHY (Ref:TED2021-129719B-C21) funded by MCIN/AEI/10.13039/501100011033 and European Union's NextGenerationEU/PRTR; and the project SHYGAS (Ref:PID2021-125812OB-C22) funded by MCIN/AEI/10.13039/501100011033 and European Union's FEDER. Computations are performed on the Tier-1 Computational Resources available at the VSC (Flemish Supercomputer Center), where an allocation of 7,300,000 CPU-hours was conceded, and on the Magerit supercomputer, managed by the Supercomputing and Visualization Center of Madrid (CeSViMa) of Universidad Politécnica de Madrid (UPM).

REFERENCES

[1] Morkovin, M. V., "Critical Evaluation of Transition from Laminar to Turbulent Shear Layers with Emphasis on Hypersonically Traveling Bodies," AFFDL-TR-68-149, Air Force Flight Dynamics Laboratory, Wright Patterson Air Force Base, Dayton, Ohio, 1969.

[2] Smith, A., and Gamberoni, A., "Transition, pressure gradient, and stability theory," Douglas Aircraft Co. Rept ES26388, 1956.

[3] Ingen, J. L. V., "A suggested semi-empirical method for the calculation of the boundary layer transition region," Univ. of Technology Delft Rep. UTH 1-74, 1956.

[4] Lin, N., Reed, H. L., and Saric, W. S., "Effect of leading-edge geometry on boundary-layer receptivity to freestream sound," Journal of Fluid Mechanics, Vol. 777, 2015, pp. 430–460.

[5] Buter, T. A., and Reed, H. L., "Boundary layer receptivity to free-stream vorticity," Physics of Fluids, Vol. 6 (10), 1994, p. 3368–3379.

[6] Schrader, L.-U., Brandt, L., Mavriplis, C., and Henningson, D. S., "Receptivity to free-stream vorticity of flow past a flat plate with elliptic leading edge," Journal of Fluid Mechanics, Vol. 653, 2010, pp. 245–271.

[7] Jacobs, R. G., and Durbin, P. A., "Simulations of bypass transition," Journal of Fluid Mechanics, Vol. 428, 2001, pp. 185–212.

[8] Brandt, L., Schlatter, P., and Henningson, D. S., "Transition in boundary layers subject to free-stream turbulence," Journal of Fluid Mechanics, Vol. 517, 2004, pp. 167–198.

[9] Mack, L. M., "Boundary layer linear stability theory," Special Course on Stability and Transition of Laminar Flow, AGARD 709, 1984.

[10] Plogmann, B., Würz, W., and Krämer, E., "Stability of a boundary layer flow in the wake of a medium height roughness element," 44th AIAA Fluid Dynamics Conference, AIAA Aviation, Atlanta, GA, 2014.

[11] Bucci, M. A., Cherubini, S., Loiseau, J.-C., and Robinet, J.-C., "Influence of free-stream turbulence on the flow over a wall roughness," Phys. Rev. Fluids, Vol. 6, 2021, p. 063903.

[12] von Doenhoff, A. E., and Braslow, A. L., "The effect of distributed surface roughness on laminar flow," Boundary layer and flow control, edited by G. V. Lachmann, Pergamon, 1961, p. 657–681.

[13] Weingärtner, A., Mamidala, S. B., and Fransson, J. H. M., "Instabilities in the wake of an isolated cylindrical roughness element," Journal of Fluid Mechanics, Vol. 960, 2023, p. A8.

[14] de Paula, I. B., W., Würz, Mendonça, M. T., and Medeiros, M. A. F., "Interaction of instability waves and a three-dimensional roughness element in a boundary layer," Journal of Fluid Mechanics, Vol. 824, 2017, pp. 624–660.

[15] de Vincentiis, L., Henningson, D. S., and Hanifi, A., "Transition in a infinite swept-wing boundary layer subject to surface roughness and free-stream turbulence," Journal of Fluid Mechanics, Vol. 931, 2022, p. A24.

[16] Schlatter, P., "Direct numerical simulation of laminar-turbulent transition in boundary layer subject to free-stream turbulence." Master's thesis, Diploma Thesis Winter Term 2000/2001, 2001.

[17] Fischer, P., Kruse, J., Mullen, J., Tufo, H., Lottes, J., and Kerkemeier, S., "NEK5000 – Open Source Spectral Element CFD solver," https://nek5000.mcs.anl.gov/index.php/mainpag, Royal Institute of Technology, 2008.

[18] Shahriari, N., "On stability and receptivity of boundary-layer flows," Tech. rep., Royal Institute of Technology. Department of Mechanics, 2016.

[19] Rodríguez, D., and Gennaro, E. M., "Three-dimensional flow stability analysis based on the matrix-forming approach made affordable," International Conference on Spectral and High-Order Methods 2016, edited by J. S. Hesthaven, Springer, 2017.

[20] Rodríguez, D., and Gennaro, E. M., "Enhancement of disturbance wave amplification due to the intrinsic three-dimensionalisation of laminar separation bubbles," The Aeronautical Journal, Vol. 123, No. 1268, 2019, pp. 1492–1507.